Identifying multiple eruption phases from a compound tephra blanket: an example of the AD1256 Al-Madinah eruption, Saudi Arabia

E. Kawabata · S. J. Cronin · M. S. Bebbington ·
M. R. H. Moufti · N. El-Masry · T. Wang

Abstract Complex eruption episodes commonly produce several phases of tephra fall and/or concurrent falls from multiple vents. Phases of eruption are challenging to reconstruct from the geological record, especially where there is a lack of distinct physical or chemical variations during an eruption episode. A statistical method is proposed for identifying the most likely combination of multiple fall lobes for composite tephra deposits, using a new high-resolution tephra fall map from the basaltic AD1256 Harrat Al-Madinah fissure eruption in Saudi Arabia. This dominantly effusive eruption episode lasted 52 days periodically producing tephra from several vents along the fissure. Most tephra was produced from high Hawaiian fountains and dispersed under differing wind conditions. The widest-dispersed tephra occurred under phases of the highest fountains, at least 500 m high and probably closer to 1000 m. These high fountains produced pyroclasts with a broad range of vesicularity. Similar total versus lobe-specific grain size determinations showed little systematic variation of maximum fountain-height phases. Individual tephra lobe properties (vesicle form, density, particle shape and particle-size distribution) in different sectors around the volcano varied only subtly. From the statistical distribution of spot fall-thickness measurements, a semi-empirical tephra fallout model, modified to account for weathering, wind remobilisation and settling, was fitted using maximum likelihood estimation. A range of likely eruption-event scenarios were evaluated, concluding that the AD1256 eruption most likely comprised three separate fall-producing eruptions from its northern vent under differing wind conditions. The first of these occurred concurrently with high-fountaining events from two other major vents southward along the fissure, producing overlapping fall lobes. Applying this method to other similar compound tephra deposits will help elucidate more realistic eruption scenarios and event reconstructions from the geological record.

Keywords Tephra · Grain size distribution · Statistical method · Volume estimation

E. Kawabata (✉) · S. J. Cronin · M. S. Bebbington
Volcanic Risk Solutions, Massey University, Private Bag 11222,
Palmerston North 4442, New Zealand
e-mail: e.kawabata@massey.ac.nz

M. R. H. Moufti · N. El-Masry
Faculty of Earth Sciences, King Abdulaziz University,
P.O. Box 80200, Jeddah 21589, Saudi Arabia

T. Wang
Department of Mathematics and Statistics, University of Otago,
P.O. Box 56, Dunedin 9054, New Zealand

Introduction

In most distributed volcanic fields, there is a lack of historically observed eruptions. Hence, hazard evaluation and eruption-scenario development relies mainly upon the interpretation of volcanic deposits. This is rather complicated when eruption episodes involve several repeated pyroclastic phases (and/or several vent areas) with similar eruption mechanisms building composite tephra aprons. Distinguishing individual tephra fall phases from composite deposits, or correlating vents with deposits (Bebbington and Cronin 2011), is only possible if there are significant stratigraphic markers, formed by changes in column height, composition, fragmentation style, wind direction, inter-event erosion or non-volcanic sedimentation. Explosive basaltic eruptions, especially Hawaiian-style fire fountaining, often show only minor variations in style or composition throughout an eruption episode; thus, complex-event stratigraphic sequences may be difficult to decipher from field examination of their tephra deposits (e.g. Parcheta et al. 2013).

The alkali basaltic AD1256 Al-Madinah eruption near Al-Madinah in Saudi Arabia (Fig. 1) formed a ~2.5-km-long roughly N–S striking fissure, with several small spatter cones and ramparts, as well as three larger scoria/cinder cones (cones 4, 5 and 6 of Camp et al. 1987). The largest cones were the source of widespread scoria lapilli (grain size terms follow White and Houghton 2006) fall deposits that extend out for several kilometers in almost all directions from the vents. Although representing <5 % of the dominantly effusive volume of this eruption, tephra >5 cm in thickness covered at least 40 km^2 and represents a significant source of hazard in future such eruptions. The AD1256 eruption took place over 52 days with at least two separate episodes of tephra fall recorded by local written records (Camp et al. 1987). Fall deposits predominantly occur below the extensive lava flows around the cones, but a few *kipukas* in the north and northwest expose tephra, and tephra covers small spatter ramparts at the south edge of the fissure that were formed in the early eruption stages. The overall eruption produced a very tight range of magma compositions, with whole-rock SiO$_2$ content ranging between 45.6 and 46.4 wt%, with greatest differences expressed in MgO content (5.6–9.3 wt%; Camp et al. 1987; Murcia et al., in review). The eruption was volumetrically dominated by lava flows (>0.3 km^3) with initially high, then low MgO-content magmas, reflecting deep fractionation of pyroxene and olivine (Murcia et al., in review). The tephra blanket was dominantly erupted in the earliest stage of the eruption, with the most primitive magmas of the narrow overall range erupted. In all rocks, phenocrysts account for <8 vol.% (corrected for vesicle volume) and comprise olivine and plagioclaise crystals 4–8 mm diameter, within in a glassy highly vesicular matrix, with rare microlites of plagioclaise.

For this study, we made 140 spot thickness measurements (excluding bomb/ballistic beds in near-vent areas and the cones) and systematically sampled the deposits. The new map (Fig. 2) confirms that tephra is dispersed in several sectors, implying that individual falls occurred at different times under diverse wind conditions. This hyper-arid terrain has little permanent vegetation cover and excellent preservation conditions for the lapilli-dominated deposits. Rare surface floods and high winds have eroded much of the outer margins of the tephra blanket, meaning that reliable measurements of falls extend to ~3 cm thickness.

Numerical forecasting of tephra fall dispersal and thickness is most commonly based on applying advection-diffusion equations within a range of eruption magnitude and grain size parameters, along with wind information (e.g. Bursik et al. 1992; Costa et al. 2006; Folch 2012). Reversing this approach, to interpolate eruption and wind parameters from tephra deposits is difficult as it is very hard to explore the parameter space in such inverse problems, and the resulting fit may not be statistically optimal (e.g. Connor and Connor 2006; Scollo et al. 2008). In addition, most commonly applied tephra fall models are scaled to eruptions of ash particles from high tephra plumes, rather than low, fire-fountaining Hawaiian eruptions. All of these methods are also challenging to apply to reconstruct likely eruption/tephra fall events under differing conditions from a composite fall deposit. An alternative approach is to use statistical techniques (e.g. Bonadonna and Costa 2012) to estimate tephra dispersal parameters in an empirical model. Kawabata et al. (2013) described a new method to do this while explicitly accounting for the variability in point measurements of tephra thickness. Parameters in the statistical dispersal model can be consistently derived through maximum likelihood estimation to extract the theoretical ideal dispersal, even with more than one fall event. In contrast to the well-described Heimaey and Ukinrek eruption sequences examined by Kawabata et al. (2013), the AD1256 Al-Madinah eruption has no detailed observations of individual timings and wind directions for each of its eruption phases, and the tephra deposits were mapped only ~750 years later. Thus, any statistical approach must first be adapted for handling weathered/compacted tephra, and a method is needed to define the most likely number of explosive/tephra fall events that constructed the composite fall blanket. The complex AD1256 eruption sequence is a case study typical of the challenges in interpreting eruption scenarios from the geologic record in basaltic environments.

Fig. 1 Oblique aerial view of the largest cones along the NNW aligned fissure system produced during the AD1256 Al-Madinah eruption

Tephra characterisation methods

A chain of up to eight vents was formed in this eruption (Camp et al. 1987), but several were <20 m high spatter cones without associated tephra blankets. Spatter and cone-flank deposits were not categorised further in this study. For the surrounding tephra blanket, spot thickness measurements were made in two periods in early 2012. Transects on foot were carried out to collect an even spatial density of sample sites. Tephra between 5 and 100 cm thick was consistently of med-fine scoria lapilli grade (>2–32 mm diameter). At each site, the tephra was excavated down to the paleo-ground

Fig. 2 Lapilli ash-fall distribution map for the AD1256 tephra blanket, with spot thickness measurements (cm) marked and automated isopachs drawn using a simple kriging process (Cleveland et al. 1992). The lava and spatter blankets are shown by the *light* and *darker grey* shading. Sample locations TS1, TS10 and TS27 referred to in the text are indicated. *Inset* map shows the position of the eruption in the Harrat Rahat, western Saudi Arabia
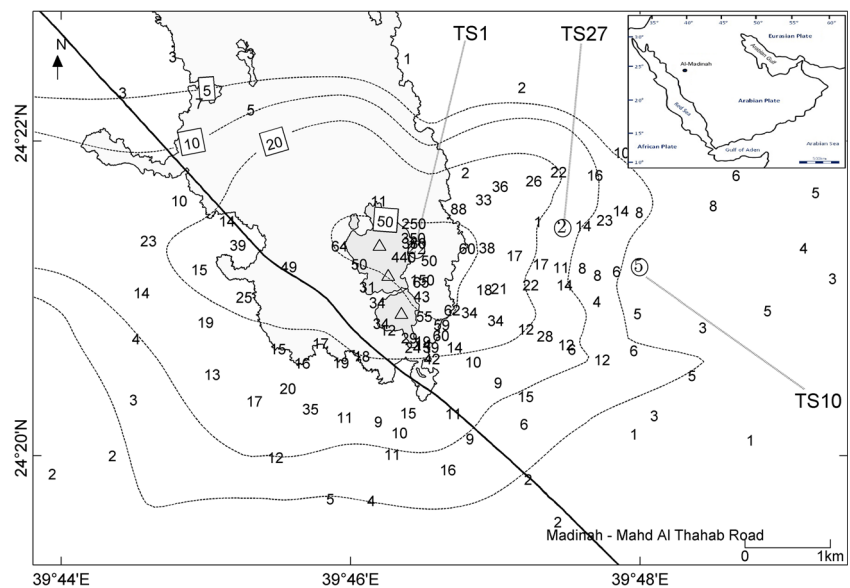
surface and, if present, reworked, or disturbed material was removed from the top. Three to four excavations were made on flat areas at each site to avoid areas of over-thickening (in hollows or against obstacles) and under-representation (e.g. on ridge crests). To ensure that only primary tephra was sampled and measured, the tephra was checked for the ubiquitous intact, but highly fragile clasts (e.g. pelee's hair, reticulite). Samples of between 0.3 and 2 kg (depending on grain size) were collected from the central portion of the deposit for sieving and laboratory textural analysis. The *d*-max (maximum diameter of the five largest clasts) was also recorded, along with a visual assessment of the main textures and any subtle vertical variations in grain size or texture. All sites show top–down penetration to 5–10 cm of pale-brown silt sourced from frequent dust storms of the area and washed down with rare rainfall events. In distal sites, with fall thicknesses of <3 cm, sheltered undisturbed sites were rare.

Little or no vertical grain size variation was observed in any one profile, and no systematic variation was seen across the whole tephra blanket (or in any one sector). Each sample was carefully hand-sieved at half-ϕ intervals to avoid further fragmentation and production of fines, although, to a certain extent, it could not be avoided in some samples, and it was noted that many coarse lapilli clasts were fragile and broke apart on sampling. Yellow, non-volcanic fine silt contaminated some of the samples, especially the finer-grained units. This was easily distinguished from the tephra and removed from the grain size distributions. A total grain size distribution for the deposit was calculated using an isopach-weighted approach following that of Parfitt (1998). Separate, isopach-weighted grain size distributions were also calculated for each sector around the vents.

Vesicularity properties were measured by sampling between 10 and 35 individual lapilli from each of the 11 selected samples

in several locations in different sectors of the tephra deposit. Each lapilli sample from the −4 to −3ϕ fraction was weighed, and bulk volumes were obtained with a Micrometrics GeoPyc 1360 envelope density analyzer (±1.1 % reproducibility). Skeletal and solid volumes were obtained with a Quantachrome Gas-Pycnometer using pure nitrogen (N_2) as the flowing gas (±0.2 % reproducibility of gas flow) with the intact followed by crushed lapilli, respectively. The instrument automatically repeats measurements on each sample until several successive determinations fall within the average standard error (σ=0.3–0.5). The combination of these measurements allows the calculation of the following volumes by difference: solid volume (as directly measured from crushed lapilli), total pore volume (difference between envelope and solid volumes), connected pore volume (difference between skeletal volume and envelope volume) and isolated pore volume (=envelope volume−skeletal volume−solid volume).

Physical and textural properties of the AD1256 Al-Madinah tephra

Explosive basaltic volcanism most commonly falls under the umbrella of Hawaiian or Strombolian eruptions (Houghton and Gonnermann 2008). The former are typically low-viscosity, mostly effusive eruptions. Hawaiian eruptions with highest magma flux and high gas contents produce distinctive fountains, which, along with feeding lava flows, also generate tephra in the cooler outer portions dispersed by winds (Head and Wilson 1989). Hawaiian fountains are mostly <100 m in height, but in some eruptions, they may reach >500 m (Houghton and Gonnermann 2008) or even >1000 m (Abe and Takahashi 1987). While Hawaiian eruptions generally produce moderately vesicular pyroclasts (>70 %), the

insulated cores of the highest plumes allow time for vesicles to grow, fragmenting particles with >90 % vesicularity and polyhedral-structured reticulite particles with >95 % vesicularity (Mangan and Cashman 1996; Parcheta et al. 2013). A common feature of these eruptions is that the fountain may vary rapidly in height over hours to days (e.g. Richter et al. 1970), but tephra fall deposits (outside the cone) may show similarities to the thinning properties of Plinian eruptions (Parfitt and Wilson 1999). Strombolian eruptions also generally involve low-viscosity basaltic magmas, but in this case, gas is often decoupled from the magma, rising through it to form explosive bursts (Blackburn et al. 1976). These produce short-lived pulsatory eruption plumes (Parfitt and Wilson 1995) and generally pyroclasts with much lower vesicularity (e.g. Polacci et al. 2006). While rare basaltic magmas produce sub-Plinian or Plinian eruptions, violent Strombolian eruptions are typically the most explosive form of activity in distributed volcanic fields (Pioli et al. 2008).

The AD1256 tephra deposit is dominated by highly vesicular equant scoria, with shiny fluidal surfaces. Common to all sites are subordinate reticulite and pelee's tears and hair. These textures are indicative of energetic Hawaiian style steady-fountain eruptions (Mangan and Cashman 1996; Parfitt and Wilson 1999). Types of fragmentation and eruption mechanisms were apparently constant throughout the tephra-production phase, which overlapped with at least some of the lava production. Along with distribution of tephra in multiple directions around the vents (Fig. 2), the maximum grain size isopleths (Fig. 3) clearly indicate fall lobes to the east and southeast, along with a poorly defined westerly lobe or lobes. There are strong contrasts in tephra grain size with distance and thickness, showing a strong fining and broadening of an initially very coarse-skewed mode (Fig. 4). The geometry of the fall deposit and the character of the scoria

indicate a Hawaiian fragmentation mechanism. The median grain size versus sorting of all samples from the AD1256 tephra deposits are consistent with basaltic fall data from other sites (Fig. 5). The common presence of reticulite clasts throughout the tephra, along with the dispersal of tephra several kilometres from the vents (Fig. 2), indicates periods of very high fountain heights, similar to energetic Hawaiian eruptions with peak fountain heights >500 m such as the 1959 Kilauea-iki event (Richter et al. 1970), which also produced a similar scale tephra blanket (Parfitt 1998). The thickness-weighted total grain size distribution of the AD1256 tephra (Fig. 6) is coarse-skewed, with particles dominantly in the fine lapilli range. The distribution is very similar (Fig. 7) to the distal portions of the 1959 Kilauea-iki tephra (excluding the cone component), which has a similar crystallinity and Silica content (but higher MgO and lower alkalis to the AD1256 magma) (MacDonald and Katsura 1961). The AD1256 pyroclastic size distribution also overlaps with the proximal portion of the deposit from the 1986 Izu-Oshima eruption, which, in addition to its climactic Plinian eruption, produced long phases of fire fountaining >1000 m high (Mannen 2006), driven by a more evolved basalt to basaltic andesite (~53 % SiO_2 and ~4.7 % MgO; Fujii et al. 1988). The Strombolian 1973 Heimaey eruption, with an almost identical composition and crystal content by comparison (Mattsson and Oskarsson 2005), shows a broader distribution than the AD1256 Al Madinah deposit, including a much greater component of fines.

Individual total grain size estimates were also calculated for different sectors around the vents in the AD1256 tephra deposit (Fig. 8). They show subtle variation among sectors, with the western fall having a greater proportion of fines (consistent with its wider dispersal) and the northeastern deposit being the coarsest.

Fig. 3 Lapilli ash-fall distribution map for the AD1256 tephra blanket, with maximum clast size marked and automated isopleths drawn using a simple kriging process (Cleveland et al. 1992). The lava and spatter blankets are shown by the *light and darker grey* shading
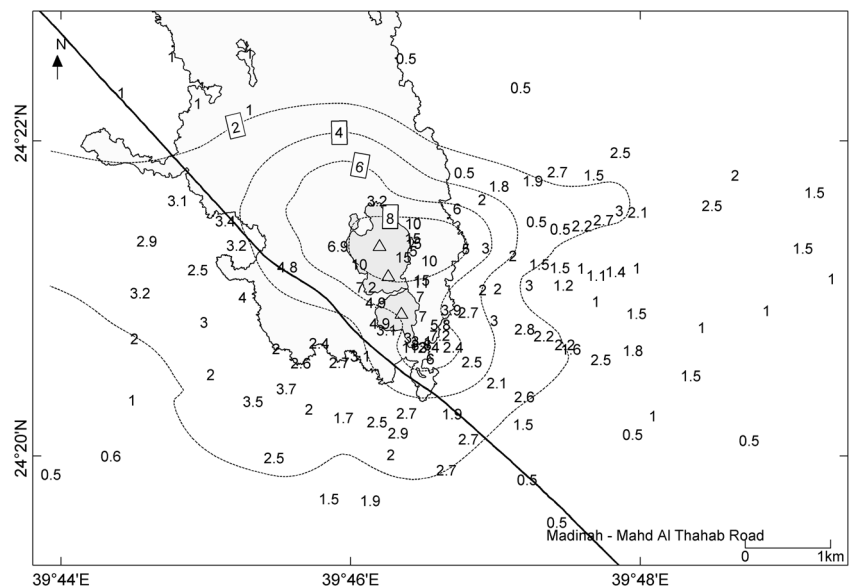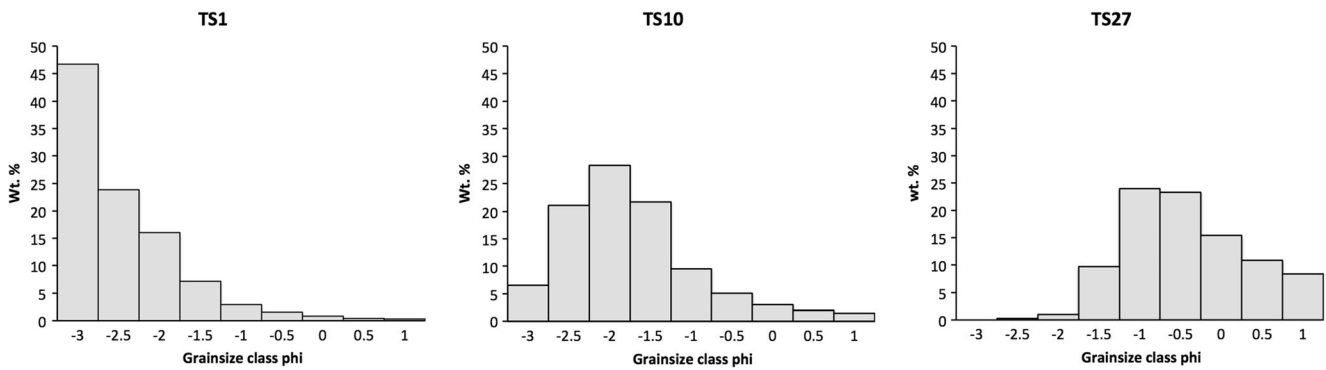
Fig. 4 Grain size distributions of AD1256 tephra from proximal (TS1, 22 cm thick, 400 m from source), medial (TS10, 5 cm thick, 2 km from source) and distal (TS27, <2 cm thick, 3.1 km from source)

The overall pyroclast density and porosity of the tephra is highly variable (Fig. 9a, b), with porosity dominated by inter-connected vesicles. The isolated porosity is the highest and shows its greatest variability at low total porosities, which is consistent with particles sourced from a range of fountain heights and from both the cool/chilled exterior of fountains as well as the central portions that experienced vesicle expansion and coalescence for longer periods (Mangan and Cashman 1996). The highest porosity clasts, with reticulite-like vesicularity, along with the presence of true reticulite clasts that are too fragile to sample and measure, indicate that very high fountains occurred during some phases of this eruption. There is a consistent trend of increasing connected porosity (and lowering variation in isolated porosity) with higher total vesicularity (Fig. 9b). This indicates a steady vesicle growth and ripening process, with the high permeability/connected porosity of polyhedral-structured vesicle networks consistent with reticulite observed in the highest Hawaiian fountains (Mangan and Cashman 1996; Parcheta et al. 2013). Comparing densities between tephra fall in different sectors around the volcano (Fig. 9a, b), while overall, the properties are similar, the

northeast and western tephra deposits show the largest range in isolated porosities and the greater proportion of lapilli with low porosity values. The wider distribution and greater isolated porosity may indicate that these lobes included deposits from Strombolian-style explosive phases (Polacci et al. 2006) to the eruption, with higher columns and more rapid chilling of pyroclasts. The eastern and southern sectors show tephra with greater proportions of highly vesicular lapilli and the lowest isolated porosity, consistent with Hawaiian style lava fountaining. The highest variability and greatest values of porosity in proximal deposits <1 km (Fig. 10) reflect the compound nature of the deposit from fountaining and explosive phases of varying intensity.

Statistical identification of fall lobes

The actual tephra thickness measured at any point differs from an 'ideal' (model) thickness due to variations in site-specific preservation and observational error. In addition, for this >750-year-old eruption, the effects of compaction and erosion

Fig. 5 Plot of median diameter vs. sorting coefficient for the measured AD1256 tephra fall samples, compared to basaltic pyroclastic fall-specific fields of the Walker and Croasdale (1972) diagram, as re-drafted by Houghton and Gonnermann (2008) using fields defined by the 1886 Tarawera high-Al basaltic Plinian fall, Crater Hill, Auckland alkali basaltic strombolian and phreatomagmatic falls and Etna and Hawaii basaltic Hawaiian fall units
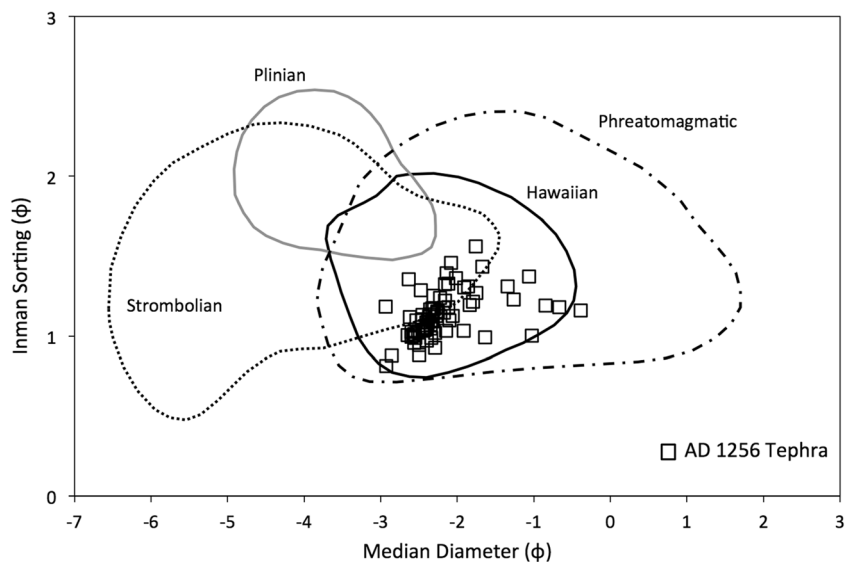
Fig. 6 Isopach-weighted total grain size distribution calculated for the AD1256 tephra deposit, showing Folk and Ward (1957) grain size parameters
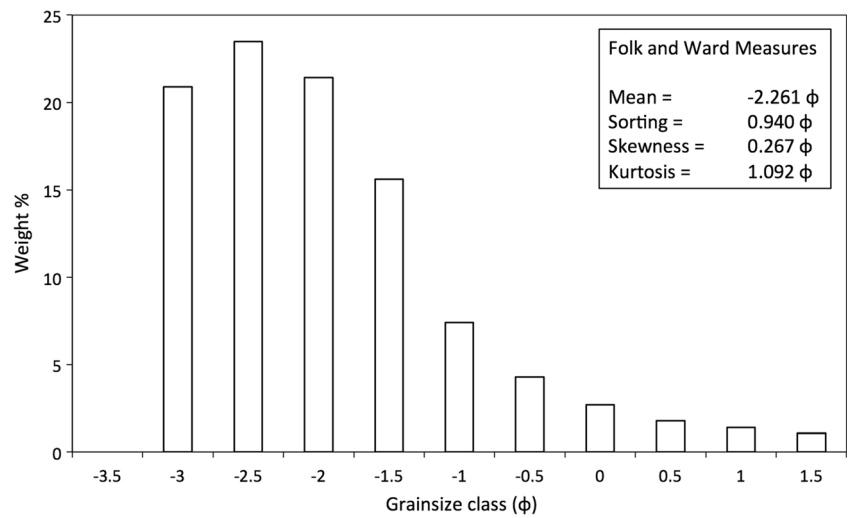

on the tephra blanket also need to be accounted for. This difference from ideal is termed the aleatory uncertainty, or sampling error, and can be explicitly incorporated in the estimation procedure. Consider the possible observed thickness, T, at a particular location has a (non-negative) probability distribution. Kawabata et al. (2013) showed that the Weibull

$$f(T) = \frac{\kappa T^{\kappa-1}}{\lambda^{\kappa}} \exp\left[-\left(\frac{T}{\lambda}\right)^{\kappa}\right], \qquad (1)$$

and the gamma

$$f(T) = \frac{T^{\kappa-1}}{\lambda^{\kappa} \Gamma(\kappa)} \exp\left(\frac{-T}{\lambda}\right), \qquad (2)$$

distributions describe this inherent variability in the tephra thickness measurements well; κ is the shape parameter, and λ the scale parameter of the respective distributions. Where Eqs. (1) and (2) differ is in the likelihood of observing unexpectedly large thicknesses. It is almost certain that for tephra $\kappa > 1$, which indicates a positive mode of the thickness distribution(s) and hence a tendency for thicknesses to be consistent with a wind and distance-decay model. By contrast, a mode at zero implies a more random deposition of tephra. Hence, Eq. (1) is less likely to produce greatly over-thickened measurements and is preferred for modelling fresh tephra observations. Considering that the AD1256 tephra has been subject to erosion and reworking for several centuries, finer grained and thinner parts of the deposit are more likely to be eroded and reworked in comparison to coarser/thicker units as noted
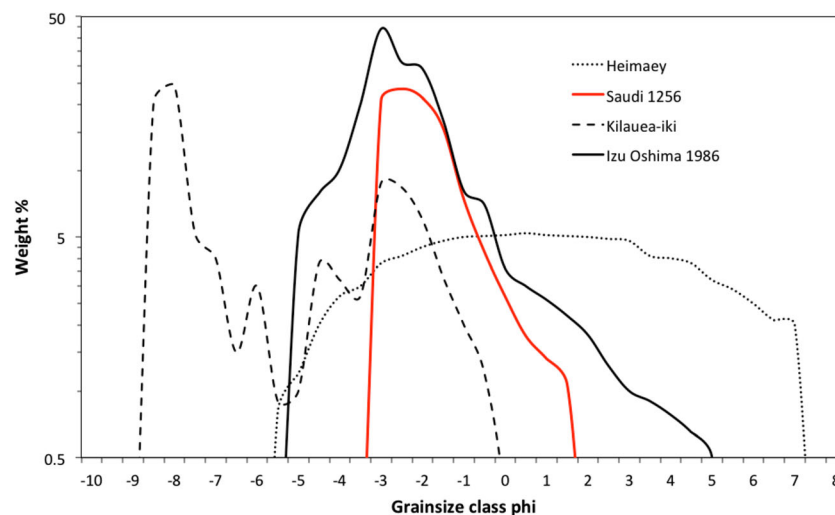
Fig. 7 Total grain size distribution of the AD1256 tephra deposit compared to that of the 1959 Kilauea-iki eruption (Parfitt 1998; note that the coarse lobe represents the spatter cone, but the finer lobe of the dispersed tephra overlaps). In addition, the distribution of the 1986 Izu-

Oshima proximal tephra (Mannen 2006), produced in part by fountain heights of >1000 m directly overlaps with the AD1256 deposit. The Strombolian fall deposit of Heimaey (Self et al. 1974) has a broad overlapping mode, but extends towards much finer ash

Fig. 8 Total grain size distributions calculated separately for tephra fall in each sector/ suspected lobe around the volcano
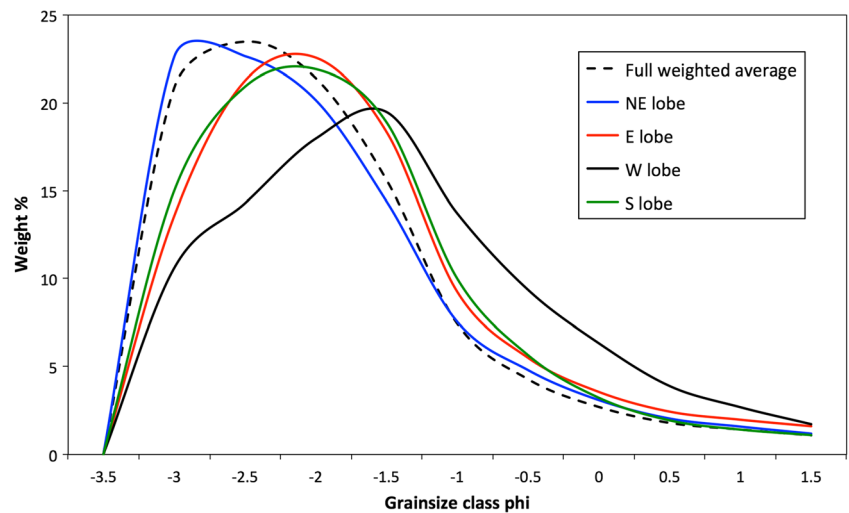

in Hawaii (Hay and Jones 1972) and during fieldwork in this study. Hence, the variability should be greatest for the outer, thinner margins of the tephra blanket. The marginal thickness behaviour is controlled by T^{κ} in both distributions, while the

greater thicknesses are controlled by $\exp[-(T/\lambda)^{\kappa}]$ in the Weibull distribution (Eq. (1)) and $\exp(-T/\lambda)$ in the gamma distribution (Eq. (2)). In the Weibull case, when thin tephra measurements disappear and κ changes, the thicker tail is lost

Fig. 9 a Isolated vs. total porosity for AD1256 lapilli particles showing those from different dispersal directions from the central vents and **b** connected vs. total porosity plotted for the same sectors/lobes
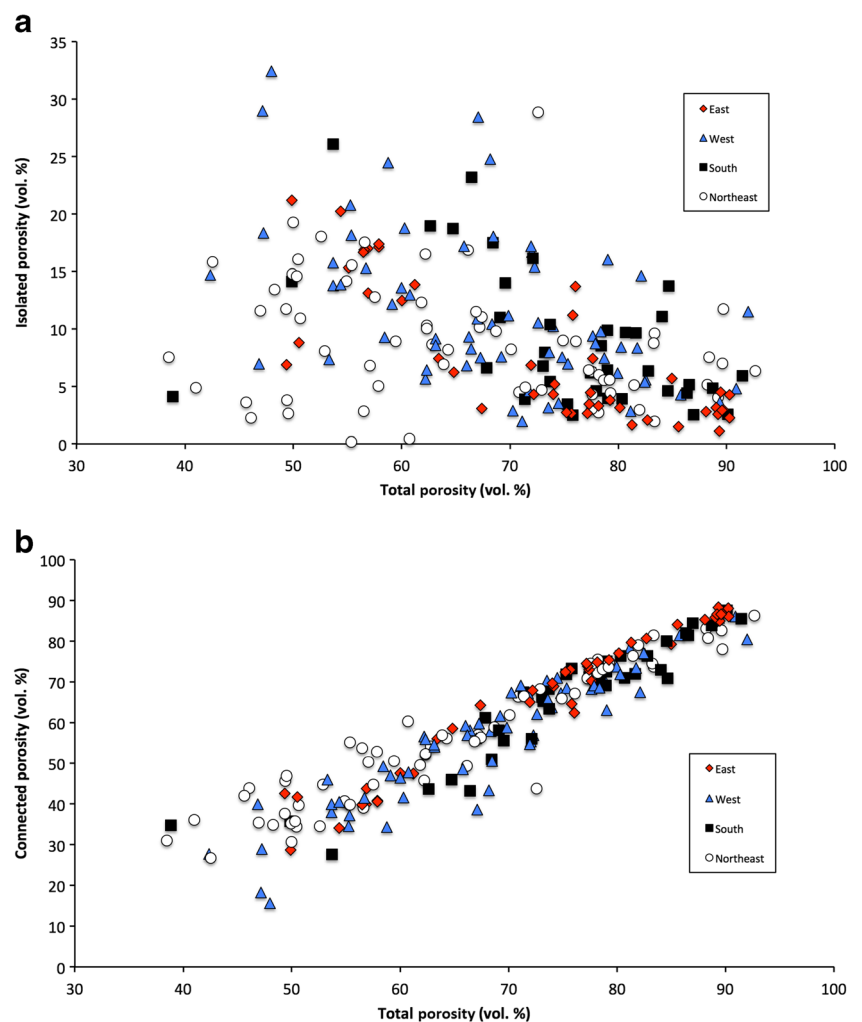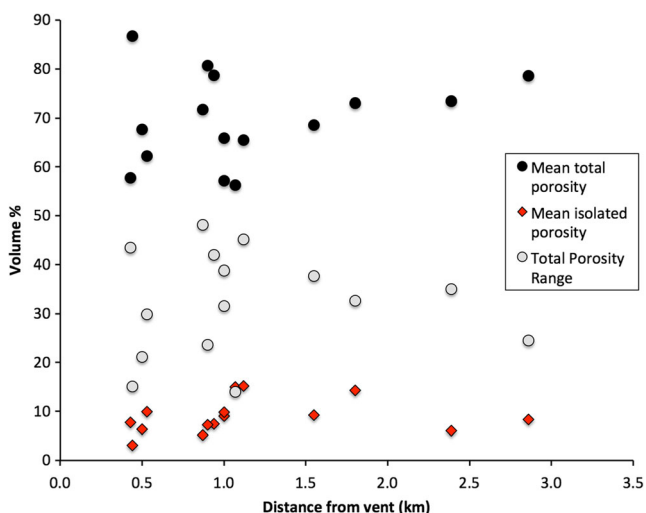
Fig. 10 Plot of mean total porosity, range in total porosity and mean isolated porosity with distance from the vent area for sample sets at each of the 15 measured sites

also due to a coupling effect. Therefore, weathering in the small measurements would remove the large measurements, contradicting reality. By contrast in the gamma distribution, the tails are independent, and there is no link between κ and λ (Fig. 11). This property means that the gamma distribution should be better suited for the description of weathered tephra deposits.

In order to test this, both the Weibull and gamma error models were fitted to the observed tephra thickness data and then used to simulate hypothetical thicknesses. The simulated data were thinned, where a tephra of thickness T disappears with a probability $\exp(-5+T/2)/[1+\exp(-5+T/2)]$; this represents a thinning probability of (0.99, 0.92, 0.5, 0.01) for deposited thicknesses of (1, 5, 10, 20) cm. The thinned data from both models, regardless of the generating model, were
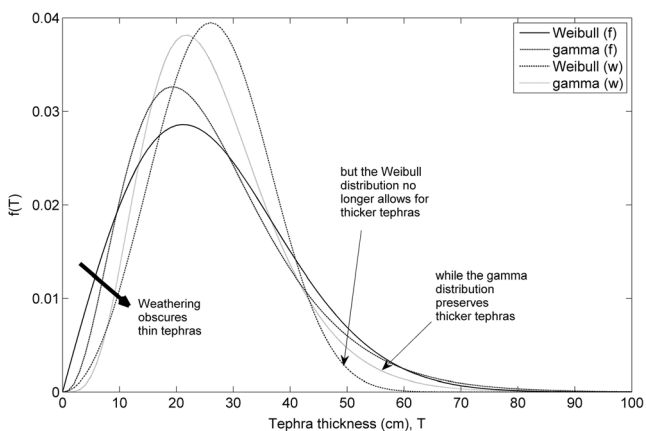
Fig. 11 Aleatory uncertainty in tephra thickness subject to weathering and compaction. The original (f) densities have the same mean and variance. The new (w) densities are then found by multiplying κ by 1.5 (to thin out the small tephras), and retaining the same mean (i.e., tephra is redispersed)

almost invariably best fitted by the gamma model. Hence, the gamma distribution was adopted for this work.

Since tephra thickness is strictly non-negative, and larger measurements will generally produce larger absolute errors, a multiplicative (aleatory) error structure is assumed, i.e., that the coefficient of variation, or relative error, in the observed thickness measurements is constant over space once the expected thickness at a given location at distance r and azimuth θ is allowed for. The latter is estimated by means of a semi-empirical attenuation relation

$$\bar{T}\ (r,\ \theta) =\ \gamma \exp\{\beta U r[1-\cos(\theta-\phi)]\}r^{-\alpha} \tag{3}$$

(Gonzalez-Mellado and De la Cruz-Reyna 2010), where the parameters include a scaling term γ (the thickness at 1 km from the source on the dispersal axis), a combination of diffusivity and wind velocity βU, which cannot be separated, the dispersal axis ϕ and the attenuation term α (Bonadonna and Houghton 2005). Fixing the expected thickness in this way replaces one of the two parameters in Eq. (2), leaving a parameter equivalent to the coefficient of variation. This is fitted, simultaneously with the parameters in Eq. (3), to the observed thicknesses using maximum likelihood estimation (MLE).

The isopach produced by Eq. (3) is an ellipse, which is the simplest geometrical approximation to most observed isopachs. Such approximation is the inevitable outcome of moving from subjective to objective isopach estimation; the former have an undefined, but arbitrarily large number of parameters that cannot be consistently estimated. The limitations of using ellipses are ameliorated by considering them as 'building blocks' from which we can construct a full isopach map. Each ellipse represents one phase of the eruption, occurring in an approximately constant wind field.

Three main vent sites produced the majority of the widely dispersed tephra. These were identified by Camp et al. (1987) and confirmed during our fieldwork, although it cannot be ruled out that small amounts of proximal tephra was produced in other locations along the fissure. Using a mixture framework, considering the total tephra thickness to be expected at a point at distance r_i and azimuth θ_i from the ith vent as

$$\bar{T}\ (r_1, r_2, r_3,\ \theta_1,\ \theta_2,\ \theta_3)$$
$$=\gamma \sum\nolimits_{i=1}^{3} \sum\nolimits_{j=1}^{n_i} P_{ij} \exp\left\{-(\beta U)_{ij} r_i\left[1-\cos\left(\theta_i-\phi_{ij}\right)\right]\right\}r_i^{-\alpha_{ij}}, \tag{4}$$

where the ith vent has n_i explosive phases, which have parameters $\gamma, P_{ij}, (\beta U)_{ij}, \phi_{ij}$ and α_{ij} in place of those in Eq. (3). This gives rise to a total of $p=4\Sigma_i n_i$ parameters because the mixing proportions P_{ij} sum to unity. This approach allows incorporation of multiple vents and lobes and can be used to identify the most likely number of eruptive stages from each

vent. The best fitting model can be identified by the Akaike Information Criterion (Akaike 1977), AIC=$2p-2\log L$, where $\log L$ is the log likelihood of the fitted model. Smaller AICs indicate better models. The AIC finds the best balance between an improved model fit and excess parameters, and thus identifies the most likely number of lobes.

Field mapping indicates that each of the three explosive vents [cones 4, 5 and 6 of Camp et al. 1987, shown in Fig. 2 as the southern vent (cone 4), central vent (cone 5) and northern vent (cone 6)] produced at least one phase of tephra fall. Hence, all combinations of eruptions were considered by adding new eruptive phases until the number of components (i.e., parameters) is no longer justified by the AIC values. Models with more than six components, besides having worsening AIC, invariably produced a component tephra fall with an infinitesimal volume. This implies that up to a maximum of six high-fountaining phases best describes the tephra dispersal of the AD1256 eruption episode. The volumes (Table 1) were numerically integrated from the fitted attenuation model (4) for each component.

Among models with the same total number of components, the best models were always those with one component on each of the middle (cone 5) and southern (cone 4) vents and the remainder on the northern vent (cone 6) (Table 1). The 4-1-1 model (four phases from cone 6, and one from each of cones 5 and 4) has the best AIC, but the improvement is only 1.0 from the 3-1-1 model. A value of 2.0 or more would indicate that the larger model is a significant improvement (Utsu 1999). Therefore, the smaller, simpler, model best describes the situation, although both are considered likely. These two models (Fig. 12) imply a series of eruptive phases of similar size, which is consistent with the similar grain size distributions, dispersal, isopleth distribution and porosity characteristics of the tephra in all dispersal directions, as described above.

Table 1 Akaike information criterion (Akaike 1977) (lowest number indicates best fit) and total bulk fall volumes of the fitted models

| Model	AIC	Total bulk fall volume (km^3)	Model	AIC	Total bulk fall volume (km^3)
1-1-1	831.7	0.017	4-1-1	812.3	0.024
2-1-1	817.0	0.021	3-2-1	816.1	0.023
1-2-1	818.2	0.020	3-1-2	817.6	0.024
1-1-2	824.7	0.022	2-3-1	822.1	0.021
3-1-1	813.3	0.021	2-2-2	822.1	0.021
2-2-1	814.8	0.020	2-1-3	825.4	0.024
2-1-2	818.1	0.023	1-4-1	825.7	0.022
1-3-1	817.7	0.022	1-3-2	825.7	0.022
1-2-2	819.2	0.022	1-2-3	827.1	0.022
1-1-3	829.3	0.025	1-1-4	837.3	0.025

Model notation is such that 4-1-1 indicates four phases on the northern vent, one at each of the middle and southern vent

The estimated total tephra volume from this eruption can be numerically integrated from the fitted attenuation model (4), yielding values of 0.021–0.024 km^3 (0.006±0.001 km^3 dense-rock equivalent—DRE). This compares favourably with the estimate using the method of Pyle (1989), as modified by Fierstein and Nathenson (1992), of 0.022 km^3 (Fig 13). The isopachs from the complete model (Fig. 12) indicate that significant fall was distributed both east and west of the vents. The largest lobes are indicated to the west and south, but these also have the greatest errors in estimation and a lack of distal sampling locations make closing the isopachs difficult. Based on the physical properties of the tephras, as described above, the northeastern and western distributed lobes were likely sourced from the highest fountains and/or the strongest winds.

Discussion

The dominant portion of the 0.5 km^3 AD1256 Al-Madinah eruption was effusive, producing lava flows that extend over 24 km from a fissure system (Camp et al. 1987). In addition, a moderately widespread tephra fall was produced. The composition, texture, grain size distribution and vesicularity properties of the AD1256 tephra implies that they were sourced from high Hawaiian-style fountains. Fissure-fed eruptions in basaltic environments typically start with fire-fountaining activity along the entire fissure length, producing little tephra. They may later transform to produce focussed, high fountains from progressively smaller numbers of vents, which generate tephra fall (Head and Wilson 1989; Parfitt and Wilson 1995; Houghton and Gonnermann 2008). Observed Hawaiian fountaining eruptions are commonly many hours, days or weeks long with rapid variations in fountain height (e.g. Richter et al. 1970; Houghton and Gonnermann 2008). The highest-fountaining phases are likely to produce the widest spread tephra under any given wind regime. Fountains over 400–500 m in height are also known to produce the most vesicular pyroclasts, with post-fragmentation vesicle growth and coalescence concentrated in their centres (Stovall et al. 2012) and high-permeability reticulite commonly produced (Mangan and Cashman 1996; Parcheta et al. 2013). Reticulite occurrence throughout the AD1256 tephras and overlapping grain size distribution properties to 1959 Kilauea-iki and 1986 Izu-Oshima tephra blankets (Fig. 7) imply that fountain heights were over 500 m. Given crater depths of >140 m in the largest vent site (cone 6), fountains would need to be >300 m for any significant tephra dispersal in the latter phases of the eruption. Hence, columns between 500 and 1000 m in height were likely reached during peak phases of the AD1256 eruption. Lower vesicularity and greater isolated porosity seen in some tephra could also imply that Strombolian eruptive phases (Polacci et al. 2006) occurred during the episode.

Fig. 12 Model component tephra lobes estimated for the AD1256 Al-Madinah eruption. **a** The 3 cm isopachs for each component of the 3-1-1 model and **b** the 4-1-1 model. The 5, 10, 20 and 50 cm isopachs are generated from the complete model. The relative (aleatory) errors at measurement locations are shown by the shape and size of symbols. *NV, MV* and *SV* denote the northern, middle and southern vents, respectively
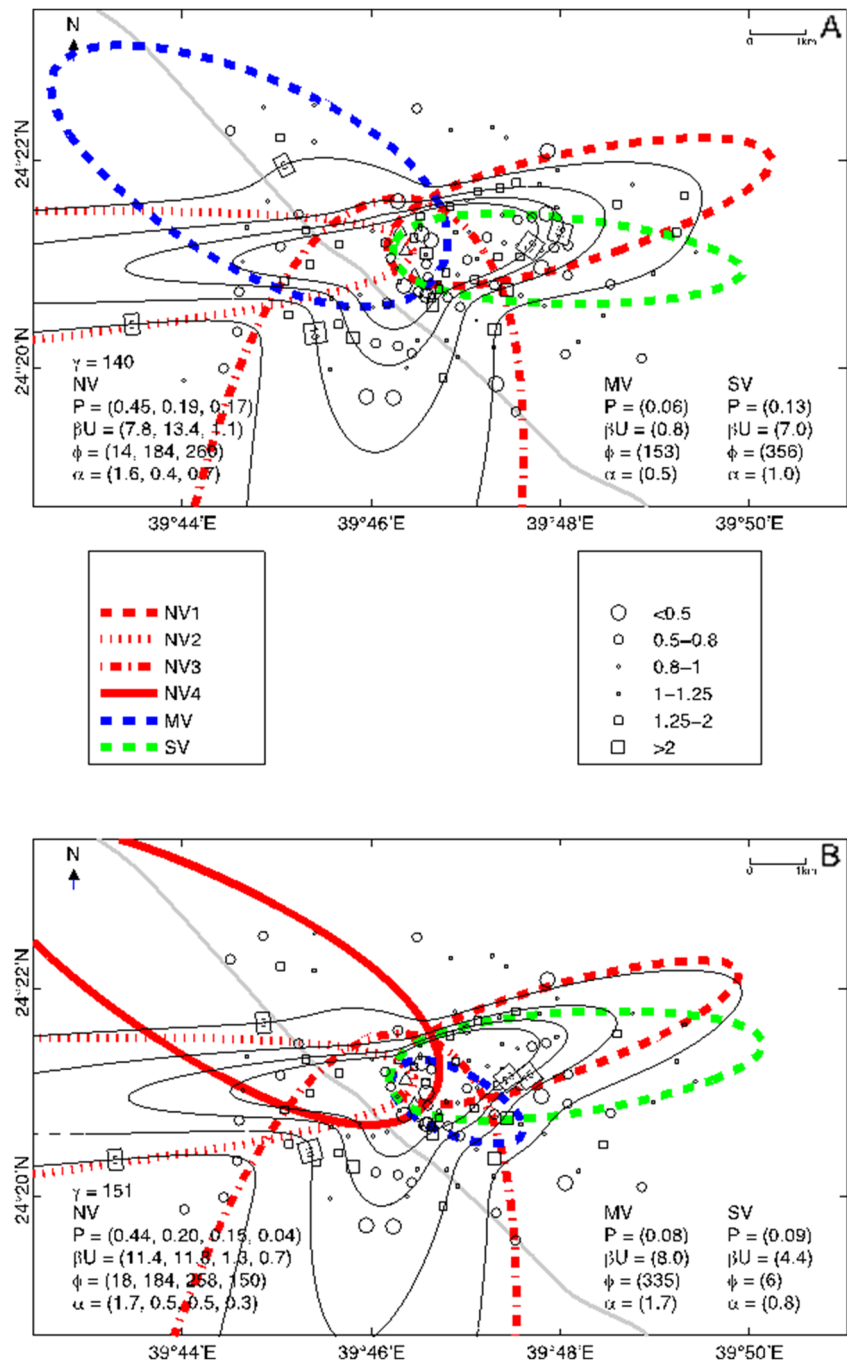

The high range in isolated porosity values for the AD1256 Al-Madinah samples probably reflects a high degree of variation in the syn-eruptive shear experienced between the margins and core of fountains. With low shear rates and low viscosity melts, bubbles may grow spherically and remain isolated (e.g. reticulite-like textures), whereas at margins of fountains, high shear may lead to stretching and mechanical coalescence of bubbles, forming the common, fluidal types of particles seen also in the deposits. The high range in all of the vesicularity properties likely reflects the high fountain heights

attained in this eruption, with large complex fountains having a range of regimes present simultaneously.

In the AD1256 eruption, historic records only describe the onset of eruption including high fire-fountaining during the first day of eruption; 'The greatest fire covered the horizon to the east of Al-Madinah' according to the translated source of Wafa Al-Wafa reported within Camp et al. (1987). This most likely indicates the initial fall being distributed eastward by westerly winds. Based on the tephra and lava stratigraphy and cone morphology, it is apparent that, of the six vents, only the
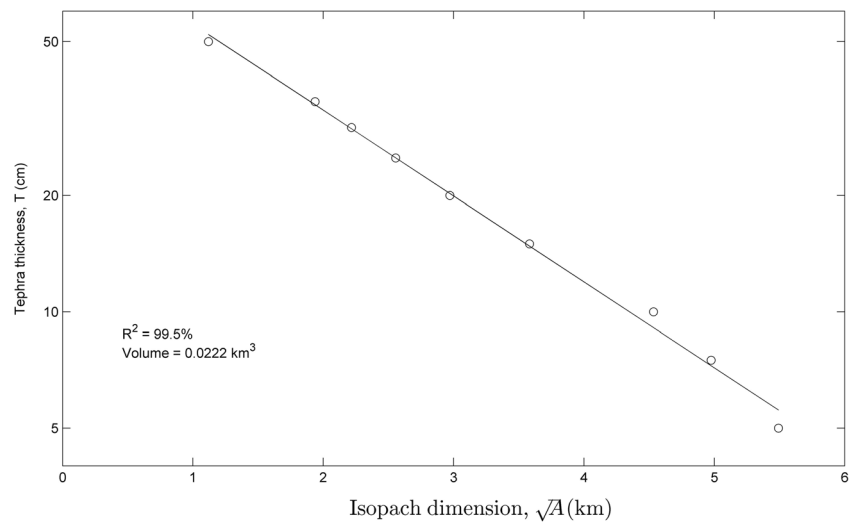
northern three [4, 5 and 6, shown in Fig. 2 as the southern vent (cone 4), central vent (cone 5) and northern vent (cone 6)] produced significant tephra. It is also apparent from the isopleth data (Fig. 3) that prominent tephra lobes from high columns were distributed to the east and southeast. Camp et al. (1987) divided the eruption up into six phases, based on chemo-stratigraphy of the lavas and tephras. All vents were probably active at the onset, but the minor cones 1–3 stopped erupting after phase II, and eruptions ceased at cone 5 after phase III. Both cones 4 and 6 erupted tephra up to and during phase V. The asymmetry of the small cone 1, with a higher rim on its eastern side, shows that westerly winds were dominant during the onset phases of the eruption, consistent with the historical descriptions. Cone 6 also has a high rim to the east, showing that westerly winds may also have been present toward the end of the eruption. Magma composition and crystallinity varied little during the eruption, remaining an alkali basalt throughout, although it was apparent that the least evolved magmas (with highest MgO contents) were erupted in the earliest phases (Murcia et al., in review).

The composite AD1256 tephra blanket (Figs. 2 and 3) extends east, west and south of the chain of cones, implying that several of the fall-producing high-fountaining events occurred on separate days under strongly differing wind directions. The statistically most likely combination of phases indicated includes either three or four periods of high-fountaining from the northern cone 6 (which is also by far the largest) with one major phase from each of the middle cone 5 and the southern cone 4. Based on the general directions indicated by the reconstructions (Fig. 12), a 4-1-1 scenario could show that high fountains occurred from vents 4–6 at the same time, with three overlapping lobes distributed generally eastward. Under the 3-1-1 scenario, the northern and southern vents (6 and 4) may have been active at the same time, due to their similar dispersal axes. Combining this information with the geological and observational records indicates that cones 4–6 probably erupted tephra during the early onset of the eruption with three overlapping lobes being deposited to the east. Two of these lobes are seen to overlap with fall directions indicated by isopleth data (Fig. 3), but isopleth data does not resolve any further specific lobes. The tephra volume erupted in this phase was between 0.0043 and 0.0049 km³ (Table 2), or between 20 and 23 % of the total. Subsequently, the major fountaining phases were centred on the northern cone 6, and possibly cone 4, distributing tephra to the south (0.0082–0.0098 km³) and east (0.0084–0.0095 km³) under differing wind directions. Present-day wind conditions at Al-Madinah (http://mesonet.agron.iastate.edu/sites/windrose.phtml?station=OEMA&network=SA_ASOS, accessed November 4, 2014) are predominantly from the west and east, corresponding well with the majority of the directions in Fig. 12. Any subsequent fountaining from cone 4 or any other vents was probably not large enough to be distinguished by the resolution of our fall data.

This statistical methodology works well for Hawaiian-style fountaining eruptions because clast-size effects are minimized, and tephra thickness is an informative measure over distances of few kilometres. To extend the method for more explosive eruptions producing high plumes, and hence wider dispersed tephra, a systematic analysis of clast-size distribution with distance is required to augment the theoretical exponential decay with distance models (Carey and Sparks 1986). Since the theoretical model produces unimodal, clast-size distributions (Sparks et al. 1992), any multimodal

Table 2 Bulk fall volumes (10⁶ m³) of each component lobe in the two favoured models

Model	NV1	NV2	NV3	NV4	MV	SV
3-1-1	2.9	4.0	8.2		4.5	1.4
4-1-1	2.5	4.1	9.8	5.4	0.6	1.8

distributions observed in the field may be best modelled by multiple eruptive phases with different column heights and/or wind directions. The resulting model will have the advantage of effectively doubling or tripling the number of observations (thickness and clast-size distribution) at the expense of additional parameters describing the clast-size attenuation. This could also be melded with field observations to determine the order of the phases. The other limitation of the method is in the calculation of total tephra volume, which is critically dependent on the estimated attenuation parameter(s). In the basaltic example here, the low columns and short dispersal distances help alleviate this problem, but some modification of the basic model (3) may be required to apply it to other settings.

Conclusions

The broad distribution of tephra surrounding the AD1256 Al-Madinah eruptive fissure shows that multiple phases of tephra fall were associated with differing wind directions during this 52-day long eruption. Based on the grain size and porosity properties, the most explosive periods of eruption involved the formation of Hawaiian fountains reaching between 500 and 1000 m in height. These high fountaining phases produced scoria with variable, but mostly high vesicularity, with >85 % porosities and reticulite clasts common in the widest spread tephras. Due to the lack of distinctive physical differences between fall lobes in different sectors surrounding the main eruptive vents, a statistical approach was developed to use spot fall thickness information to distinguish the multiple overlapping tephra lobes. This method can be used to distinguish the main tephra-producing phases produced during any similar multi-event and multi-source explosive basaltic eruption. The most likely sequence of tephra-fall phases could be identified for the AD1256 eruption including their most likely individual magnitudes. This information provides greater resolution to future tephra hazard models for this area.

With the incorporation of the gamma error distribution for the description of tephra deposits, to make it robust to thinning and erosion, this statistical model explicitly accounts for uncertainties in a preserved tephra blanket, previously a major obstacle to reconstruction of unobserved eruptions (Biass and Bonadonna 2011). It also avoids the necessity of using modern-day wind profiles, the limitations of which are discussed by Johnston et al. (2012). Moreover, the results can be integrated with physical observations to better describe the eruption.

Beyond reconstructing the dynamics of unobserved eruptions, the methodology is a building block in the development of tephra hazard models. These could take the form of a convolution of present-day wind profiles and a Bayesian hierarchical model for the number and location of vents, the number of high-fountaining periods per vent and the

parameters in the model described by Eq. (4). Understanding the total number of erupted phases of past eruptions is a key input into developing realistic emergency management scenarios for future eruptions. The next step required is to fit the model to sufficient tephra data to inform the Bayesian procedure.

Appendix

Assume $T \sim$ gamma (κ, λ) where κ is the shape parameter and λ is the scale parameter. Then, $\mu = \kappa\lambda$ and $\sigma = \sqrt{\kappa}\lambda$ by definition. Thus, $\mu = T_i(r_i, \theta_i)$ for the ith observation, and $\lambda_i = T_i/\kappa$. Note that the scale parameter is no longer a constant as it varies for each observation. The log likelihood function for the complete sample T_i ($i = 1, 2, \ldots, n$) is then obtained from Eq. (4) as $\log L = (\kappa - 1)\sum_{i=1}^{n}\log T_i - \kappa\sum_{i=1}^{n}\log\lambda_i - n\log\Gamma(\kappa) - \sum_{i=1}^{n}\frac{T_i}{\lambda_i}$

and the coefficient of variation is

$$CV = \frac{\sigma}{\mu} = \frac{\sqrt{k}\lambda_i}{k\lambda_i} = \frac{1}{\sqrt{k}}.$$

References

Abe K, Takahashi M (1987) Description of the November 21, 1986 fissure eruption on the caldera floor of Izu-Oshima volcano, Japan: analysis of a series of photographs. Bull Earthquake Res Inst 62: 149–162 (in Japanese with English abstract)

Akaike H (1977) On entropy maximization principle. In: Krishnaiah PR (ed) Applications of statistics. North Holland, Amsterdam, pp 27–41

Bebbington M, Cronin SJ (2011) Spatio-temporal hazard estimation in the Auckland Volcanic Field, New Zealand, with a new event-order model. Bull Volcanol 73:55–72

Biass S, Bonadonna C (2011) A quantitative uncertainty assessment of eruptive parameters derive from tephra deposits: the example of two large eruptions of Cotopaxi volcano, Ecuador. Bull Volcanol 73:73–90

Blackburn EA, Wilson L, Sparks RSJ (1976) Mechanisms and dynamics of Strombolian activity. J Geol Soc 132:429–440

Bonadonna C, Costa A (2012) Estimating the volume of tephra deposits: a new simple strategy. Geology 40:415–418

Bonadonna C, Houghton BF (2005) Total grain-size distribution and volume of tephra-fall deposits. Bull Volcanol 67:441–456

Bursik MI, Sparks RSJ, Gilbert JS, Carey SN (1992) Sedimentation of tephra by volcanic plumes: I. Theory and its comparison with a

study of the Fogo A plinian deposit, Sao Miguel (Azores). Bull Volcanol 54:329–344

Camp VE, Hooper PR, Roobol MJ, White DL (1987) The Madinah eruption, Saudi Arabia: magma mixing and simultaneous extrusion of three basaltic chemical types. Bull Volcanol 49:489–508

Carey SN, Sparks RSJ (1986) Quantitative models of the fall-out and dispersal of tephra from volcanic eruption columns. Bull Volcanol 48:127–141

Cleveland WS, Grosse E, Shyu MJ (1992) Local regression models. In: Chambers JM, Hastie T (eds) Statistical models in S. Chapman and Hall, New York, pp 309–376

Connor LJ, Connor CB (2006) Inversion is the key to dispersion: understanding eruption dynamics by inverting tephra fallout. In: Mader HM, Coles SG, Connor CB, Connor LJ (eds) Statistics in volcanology, vol 1. The Geological Society, London, pp 231–242

Costa A, Macedonio G, Folch A (2006) A three-dimensional Eulerian model for transport and deposition of volcanic ashes. Earth Planet Sci Lett 241:634–647

Fierstein J, Nathenson M (1992) Another look at the calculation of tephra fallout volumes. Bull Volcanol 54:156–167

Folch A (2012) A review of tephra transport and dispersal models: evolution, current status, and future perspectives. J Volcanol Geotherm Res 235–236:96–115

Folk RL, Ward WC (1957) Brazos River bar: a study in the significance of grainsize parameters. J Sediment Petrol 27:3–26

Fujii T, Aramaki S, Kaneko T, Ozawa K, Kawanabe Y, Fukuoka T (1988) Petrology of the lavas and ejecta of the November, 1986 eruption of Izu-Oshima volcano (in Japanese with English abstract). Bull Volcanol Soc Jpn 33:S234–S254

Gonzalez-Mellado AO, De la Cruz-Reyna S (2010) A simple semi-empirical approach to model thickness of ash-deposits for different eruption scenarios. Nat Hazards Earth Syst Sci 10:2241–2257

Hay RL, Jones BF (1972) Weathering of basaltic tephra on the island of Hawaii. Geol Soc Am Bull 83:317–332

Head JW III, Wilson L (1989) Basaltic pyroclastic eruptions: influence of gas release patterns and volume fluxes on fountain structure, and the formation of cinder cones, spatter cones, rootless flows, lava ponds and lava flows. J Volcanol Geotherm Res 37:261–271

Houghton BF, Gonnermann HM (2008) Basaltic explosive volcanism: constraints from deposits and models. Chem Erde 68:117–140

Johnston EN, Phillips JC, Bonadonna C, Watson IM (2012) Reconstructing the tephra dispersal pattern from the Bronze Age eruption of Santorini using an advection-diffusion model. Bull Volcanol 74:1485–1507

Kawabata E, Bebbington MS, Cronin SJ, Wang T (2013) Modeling thickness variability in tephra deposition. Bull Volcanol 75:738. doi:10.1007/ s00445-013-0738-x

MacDonald GA, Katsura T (1961) Variations in the Lava of the 1959 eruption in Kilauea Iki. Pac Sci 14:358–369

Mangan MT, Cashman KV (1996) The structure of basaltic scoria and reticulite and inferences for vesiculation, foam formation, and fragmentation in lava fountains. J Volcanol Geotherm Res 73:1–18

Mannen K (2006) Total grainsize distribution of a mafic subplinian tephra, TB-2, from the 1986 Izu-Oshima eruption, Japan: an estimation based on a theoretical model of tephra dispersal. J Volcanol Geotherm Res 155:1–17

Mattsson HB, Oskarsson N (2005) Petrogenesis of alkali basalts at the tip of a propagating rift. Evidence from the Heimaey Volcanic Centre, south Iceland. J Volcanol Geotherm Res 147:245–267

Parcheta CE, Houghton BF, Swanson DA (2013) Contrasting patterns of vesiculation in low, intermediate, and high Hawaiian fountains: a case study of the 1969 Mauna Ulu eruption. J Volcanol Geotherm Res 255:79–89

Parfitt EA (1998) A study of the clast size distribution, ash deposition and fragmentation in a Hawaiian-style volcanic eruption. J Volcanol Geotherm Res 84:197–208

Parfitt EA, Wilson L (1995) Explosive volcanic eruptions—IX. The transition between Hawaiian-style lava fountaining and Strombolian explosive activity. Geophys J Int 121:226–232

Parfitt EA, Wilson L (1999) A Plinian treatment of fallout from Hawaiian lava fountains. J Volcanol Geotherm Res 88:67–75

Pioli L, Erlund W, Johnson E, Cashman K, Wallace P, Rosi M, Delgado Granados H (2008) Explosive dynamics of violent Strombolian eruptions: the eruption of Parícutin Volcano 1943–1952 (Mexico). Earth Planet Sci Lett 271:359–368

Polacci M, Corsaro RA, Andronico D (2006) Coupled textural and compositional characterization of basaltic scoria: insights into the transition from Strombolian to fire fountain activity at Mount Etna, Italy. Geology 34:201–204

Pyle DM (1989) The thickness, volume and grainsize of tephra fall deposits. Bull Volcanol 51:1–15

Richter DH, Eaton JP, Murata KJ, Ault WU, Krivoy HL (1970) Chronological narrative of the 1959–60 eruption of Kilauea volcano, Hawaii. US Geological Survey Professional Paper 537-E: 73

Scollo S, Folch A, Costa A (2008) A parametric and comparative study of different tephra fallout models. J Volcanol Geotherm Res 176:199–211

Self S, Sparks RSJ, Booth B, Walker GPL (1974) The 1973 Heimaey Strombolian scoria deposit, Iceland. Geol Mag 111:539–548

Sparks RSJ, Bursik MI, Ablay GJ, Thomas RME, Carey SN (1992) Sedimentation of tephra by volcanic plumes. Part 2: controls on thickness and grain-size variations of tephra fall deposits. Bull Volcanol 54:685–695

Stovall WK, Houghton BF, Hammer JE, Fagents SA, Swanson DA (2012) Vesiculation of high fountaining Hawaiian eruptions: episodes 15 and 16 of 1959 Kīlauea Iki. Bull Volcanol 74: 441–455

Utsu T (1999) Representation and analysis of the earthquake size distribution: a historical review and some new approaches. Pure Appl Geophys 155:509–535

Walker GPL, Croasdale R (1972) Characteristics of some basaltic pyroclastics. Bull Volcanol 35:303–317

White JDL, Houghton BF (2006) Primary volcaniclastic rocks. Geol Soc Am Bull 34:677–680